Formation of surface magic clusters: a pathway to monodispersed nanostructures on surfaces

2001 J. Phys.: Condens. Matter 13 R589

(http://iopscience.iop.org/0953-8984/13/31/201)

INSTITUTE OF PHYSICS PUBLISHING JOURNAL OF PHYSICS: CONDENSED MATTER

J. Phys.: Condens. Matter **13** (2001) R589–R618 PII: S0953-8984(01)09093-2

TOPICAL REVIEW

Formation of surface magic clusters: a pathway to monodispersed nanostructures on surfaces

Y L Wang[1,2] **and M Y Lai**[1]

[1] Institute of Atomic and Molecular Sciences, Academia Sinica, PO Box 23-166, Taipei, Taiwan, Republic of China
[2] Department of Physics, National Taiwan University, Taipei, Taiwan, Republic of China

E-mail: ylwang@pub.iams.sinica.edu.tw

Received 17 April 2001
Published 19 July 2001
Online at stacks.iop.org/JPhysCM/13/R589

Abstract

Surface magic clusters (SMC) are clusters exhibiting enhanced stability at certain sizes on a particular surface. Through the formation of SMC, it is possible to grow an ensemble of nanostructures on a particular surface with extremely narrow size dispersion. Such monodispersed nanostructures are highly desirable for the realization of some emerging nanotechnology. This review summarizes the recent experimental observations and current theoretical understanding of SMC and discusses the possibility of exploiting the formation of such unusual clusters as a pathway to the growth of monodispersed nanostructures on surfaces.

1. Introduction

Due to their fundamental interest and almost unlimited potential applications, nanostructures have become a class of objects intensively studied by scientists and engineers around the world. It is very likely that this intensive effort will continue until the fabrication of nanostructures with atomic scale precision can be performed routinely. One of the most important steps towards this 'ultimate fabrication' is that of being able to control the number and configuration of all the atoms in the desired nanostructures as well as their environment. Although lithographic techniques based on photon, electron or ion beams have been employed for the fabrication of structures with $\sim$10 nm lateral resolution, the intrinsic limitations of these so called 'top-down' fabrication techniques appear increasingly insurmountable as the lateral dimension of the desired nanostructure becomes smaller [1]. Recent employment of scanning probe microscopes (SPM) as lithographic tools has revealed exciting possibilities for atom manipulation [2, 3]. However, the intrinsic slow speed of such serial writing methods presents serious challenges to the researchers who are attempting to develop SPM-based lithography into a practical technology. An alternative 'bottom-up' approach, based on self-assembly of nanostructures from their constituent atoms or molecules, is conceptually attractive because of its intrinsic parallel-processing nature [4–7]. In principle, a large quantity of the desired

nanostructure can be synthesized at one time. However, the size and atomic structure of such self-assembled nanostructures still suffer from relatively large variation in most cases and the spatial arrangements of the nanostructures are hard to control. Nanostructures with less than a few per cent dispersion in the distribution of their linear dimensions and/or ordering in their spatial arrangement are achieved only in a few cases [8]. Therefore, any method or concept for improving the size or structural uniformity of nanostructures, or the precision in their spatial arrangement, is important for the realization of the emerging nanotechnology.

Because of their precise control over the amount of deposited material, vacuum thin-film deposition techniques such as molecular beam epitaxy (MBE) [9] and cluster deposition [10, 11] have been employed for the growth of nanostructures on surfaces. By controlling the deposition flux, temperature and time as well as the post-deposition annealing procedure, these techniques can set the mean size (S_{avg}) of some desired nanostructures approximately at a certain desired value. For clarity and consistency, we define the size of a nanostructure as its total number of atoms rather than its characteristic linear dimension as adopted by many authors. The size dispersion ΔS (full width at half-maximum in the size distribution curve) of nanostructures fabricated by deposition of materials onto surfaces is usually larger than $S_{avg}/2$. Significant reduction in ΔS for some nanostructures has been demonstrated in certain systems by exploiting the strain on the substrate surface or in the nanostructures [12–14]. Nevertheless, the values of $\Delta S/S_{avg}$ are still larger than desired for many fundamental studies and technological applications. Therefore, developing methods for effectively reducing ΔS remains one of the most important issues for the fabrication of nanostructures on surfaces.

Magic clusters in free space have been known of for almost two decades [15, 16]. Their enhanced stability at certain sizes originates from either the electronic or atomic shell closure. Intuitively, it would seem that such especially stable clusters could be exploited for the growth of nanostructures on surfaces with narrow size dispersion. However, the shell closure of a magic cluster is hard to maintain during the landing on a surface because of the usually strong cluster–surface interaction. Although the loss of the special stability could in principle be avoided by careful selection of the cluster–surface combination [17], the SMC [18–20] discovered recently were formed via the self-assembly of adsorbed atoms (adatoms) rather than deposition of free magic clusters onto surfaces. These discoveries have raised interesting basic questions regarding the origin of the enhanced stability of SMC as well as practical issues regarding their potential applications. Although the research on this subject is still in its infancy, the formation of SMC appears to suggest a potential new pathway to the growth of monodispersed nanostructures with well-defined atomic configurations on a particular surface. In this review, we provide a brief summary of the highlights of the experimental observations and theoretical understanding of SMC, and attempt to point out some issues concerning the formation of SMC as a pathway to the fabrication of monodispersed nanostructure surfaces.

2. Experimental observations of SMC

Although speculations about the existence of magic clusters on surfaces were raised in a paper in 1992, which was based on a study of the Pt/Pt(111) surface using He scattering [21], no SMC were found in the later scanning tunnelling microscopy (STM) study of this surface [22]. The first demonstration of surface clusters exhibiting enhanced stability and abundance had to wait for several years until SMC were directly observed on the $\sqrt{3} \times \sqrt{3}$R30°-reconstructed Ga/Si(111) surface [18, 23]. Soon after this work, Si islands with magic numbers of unit cells on the Si(111) 7×7 surface were reported [19]. This was then followed by the observation of a type of Si magic cluster on Si(111) [20]. In this section, we review the highlights of these pioneering experiments and their implications for the formation of SMC on other systems.

2.1. Ga/Si(111)

The Ga/Si(111) surface has been studied extensively since the 1980s [24–31]; however, SMC have never been observed in this system. The early studies of Ga-induced reconstruction of the Si(111) surface led to two important observations. First, deposition of ∼1/3 monolayer (ML) (1 ML $= 7.83 \times 10^{14}$ Ga cm^{-2}) of Ga and subsequent annealing at ∼550 °C led to the formation of a $\sqrt{3} \times \sqrt{3}$R30°-reconstructed surface lattice (henceforth referred to as the adatom lattice). Detailed STM and x-ray standing-wave (XSW) examinations [31] unambiguously determined that the position of the Ga is on the fourfold-coordinated site (T_4), rather than the threefold hollow site (H_3) that was once intuitively assigned as the more stable position. It is to be noted that the STM image of the $\sqrt{3} \times \sqrt{3}$R30°-reconstructed Ga/Si(111) surface exhibits a mosaic pattern as shown in figure 1, indicating that the atoms occupying the T_4 sites are a mixture of Ga and Si. The contrast of the image reverses with the change in the polarity of the tip bias. Qualitatively, a Si atom at a T_4 site appears brighter in the filled-state (positive-tip-bias) image as expected, because it has one remaining dangling bond. Similar mosaic patterns have been observed on the Al-induced $\sqrt{3} \times \sqrt{3}$R30°-reconstructed Si(111) surface [32]. The coexistence of Ga and Si at the T_4 sites is also consistent with the fact that ∼1/6 ML, rather than 1/3 ML, of Ga is enough to induce the $\sqrt{3} \times \sqrt{3}$R30° reconstruction. As will be explained later, the existence of Si adatoms at T_4 sites turns out to be an important factor in the formation of SMC on the Ga/Si(111) surface. The second important observation is that the deposition of ∼1 ML of Ga and subsequent annealing at 300–500 °C result in the formation of quasi-ordered layers of hexagonally close-packed aggregates, referred to as supercells (superlattice unit cells) [28]. These supercells with the lateral dimension of 2.4 nm were identified with the 6.3 × 6.3 incommensurate structure originally observed by means of reflection high-energy electron diffraction (RHEED) [24]. Detailed XSW studies indicated that, for the 6.3 × 6.3 incommensurate structure, Ga substitutes for Si in the outer half of the Si(111) bilayer at the surface and forms a graphite-like Ga–Si bilayer [27].

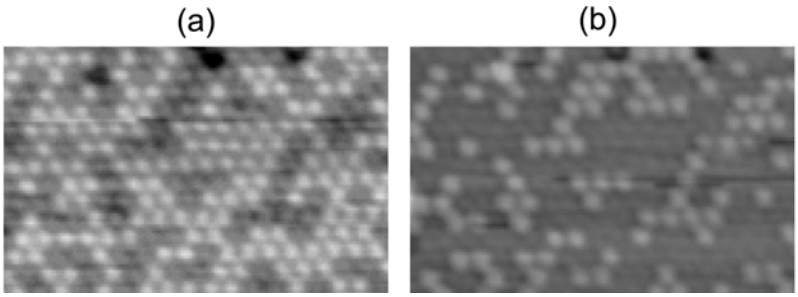

Figure 1. STM images of $\sqrt{3} \times \sqrt{3}$R30°-reconstructed Si(111) surface induced by ∼0.2 ML of Ga deposition showing a mosaic pattern (size = 8.5 nm × 13 nm). (a) Empty state ($V_{tip} = -2.3$ V, $I_t = 1.8$ nA); (b) filled state ($V_{tip} = 2.3$ V, $I_t = 1.0$ nA). Note the contrast reversal between (a) and (b).

In retrospect, we think that SMC were not observed in the Ga/Si(111) system in the previous studies because of the inadequate Ga deposition and thermal processes, in which the total amount of Ga was always deposited in a single step onto the Si(111) surface while the sample was held at low (25 °C) or high (350 °C–550 °C) temperatures. For low-temperature depositions, samples were post-annealed at high temperatures in order to achieve the ordered or quasi-periodic reconstruction of the surface. Such a single-step deposition process tends to convolute many complicated atomic processes and hamper a detailed observation of the

initial cluster formation process. In the experiment leading to the first observation of SMC, the Ga was deposited using a two-step process. First, ∼1/3 ML of Ga was deposited onto the Si(111) substrate at room temperature and the sample was annealed at 550 °C for ∼10 s to achieve a uniform $\sqrt{3} \times \sqrt{3}$R30°-reconstructed surface. Then, an additional ∼1/6 ML of Ga was deposited again at room temperature and followed by a series of annealings (∼10 s) at temperatures between 100 and 300 °C. After the second Ga deposition and prior to the annealing, vacancies and irregular droplets were formed on the adatom lattice simultaneously as shown in figure 2. Annealing of the sample at ∼200 °C led to the healing of the adatom lattice as well as the formation of ordered clusters and incommensurate islands [23], as shown by the typical filled- and empty-state STM images in figures 3(a) and 3(b) respectively. The circled clusters in the figures are examples of the most abundant SMC.

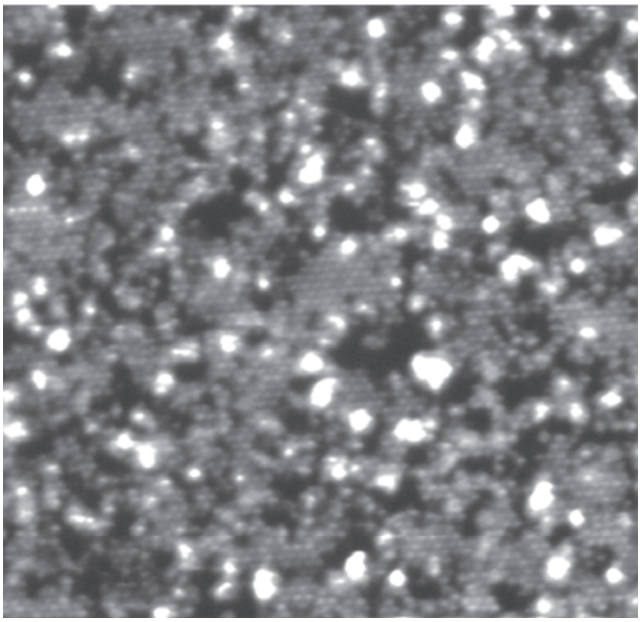

Figure 2. A STM empty-state image of Ga-induced droplets and vacancies formed on a $\sqrt{3} \times \sqrt{3}$R30°-reconstructed Ga/Si(111) surface after ∼1/6 ML of Ga was deposited ($V_{tip} = -2.1$ V, $I_t = 1.6$ nA, size = 40 nm × 40 nm).

Figure 4 shows the histogram of the clusters on the Ga/Si(111) surface prepared by the process described above. There were four species exhibiting enhanced abundance and therefore stability. These similar triangular clusters had n (2, 3, 4 or 5) atoms on their sides. The most abundant species was the $n = 4$ clusters, which made up ∼50% of the number of counted clusters and covered ∼2% of the surface area. (Depending on variations in the sample preparation process, particularly the Si concentration in the original $\sqrt{3} \times \sqrt{3}$R30° adatom lattice and the additional Ga dosage, the area coverage of the $n = 4$ clusters can be increased by a factor of two to three.) The other three more abundant species appeared primarily on the boundary of the three degenerate $\sqrt{3} \times \sqrt{3}$R30° domains and areas with higher concentrations of defects on the adatom lattice. Due to the discrete nature of cluster size, the conventional definition of size dispersion is not adequate for describing the spread of the size distribution of the clusters. The $n = 4$ SMC in this system have the same size as well as atomic structure, and their value of ΔS is essentially zero.

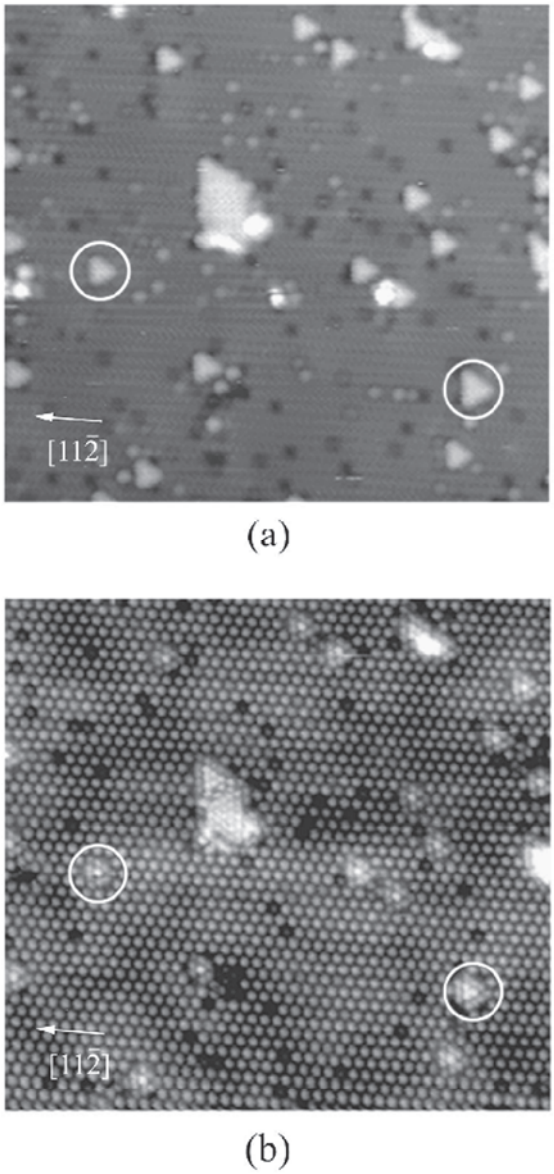

Figure 3. (a) Filled-state ($V_{tip} = 1.6$ V, $I_t = 1.8$ nA) and (b) empty-state ($V_{tip} = -1.6$ V, $I_t = 1.8$ nA) STM images (size = 29.2 nm × 27.7 nm) of Ga-induced magic clusters within the $\sqrt{3} \times \sqrt{3}$R30°-reconstructed Ga/Si(111) surface.

The atomic structures of the $n = 4$ clusters were partially revealed by the atomic resolution STM images and the corresponding tip-height profiles shown in figure 5. The centre atom is exactly above a T_4 site belonging to the original adatom lattice and the three vertex atoms also appear to be above the original T_4 sites of the adatom lattice, but with slight (∼0.11 nm) outward deviation. The six edge atoms are approximately above the degenerate T_4 sites that do not belong to the original adatom lattice, and also with some (∼0.07 nm) outward deviation. Collectively, the lateral positions of the ten observed atoms of this cluster assume

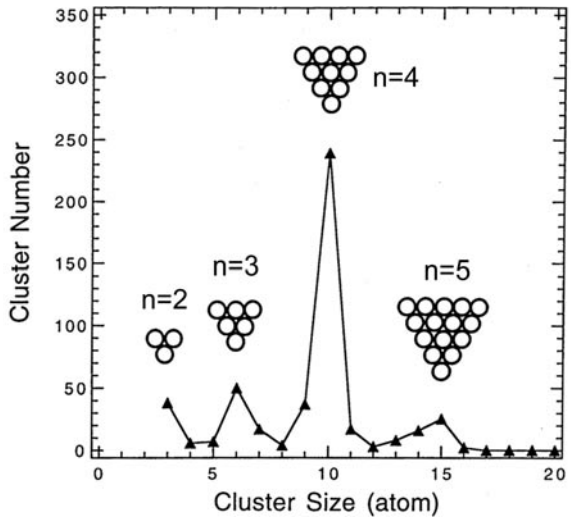

Figure 4. The histogram of the clusters within the $\sqrt{3} \times \sqrt{3}$R30°-reconstructed Ga/Si(111) surface showing the existence of magic numbers. The statistics are derived from many atomically resolved STM images covering $\sim(140\ \text{nm})^2$.

an approximate 1×1 construction with respect to the underlying Si(111) surface. Although STM tip-height profiles do not usually provide accurate measurements of the heights of the surface atoms, they can still provide some rough estimates. As measured from the empty-state and filled-state tip-height profiles across the cluster, the centre atom appears to be higher than its surrounding adatoms by ∼0.07 nm (profile A) and ∼0.12 nm (profile C), respectively. The empty-state profile also shows that the vertex atoms appear to be at the same level as the adatoms. A distinct feature of the surroundings of this cluster is to be noted: three adatoms are missing from its surrounding adatom lattice, as indicated by the triangles in figure 5(a). This characteristic vacancy pattern provides a signature for relating the SMCs to the larger clusters and incommensurate islands.

Figure 6(a) shows an example of an incommensurate island separated by dislocation into three domains. In each domain, the atoms appear to be above T_4 sites and assume an approximate 1×1 structure. The profile A of figure 6(b) shows that the interior atoms of the island appear to be ∼0.07 nm higher than the adatoms while the edge atoms appear to be at approximately the same level as the adatoms. As marked by the triangles in figure 6(a), the island's surrounding adatom lattice exhibits a vacancy pattern similar to that observed around the $n = 4$ SMC. The above structural similarities suggest that this island would be categorized as a SMC with $n = 10$, provided that its dislocations were ignored. The presence of dislocations on this island and other larger incommensurate islands with similar structure [23] indicates that the lattice constants of the Ga-induced clusters and islands are mismatched with the Si(111) surface. As their lateral dimensions grow beyond a certain limit (5–7 lattice units in this system), elastic strain alone cannot cope with the stress and dislocations are created to reduce the stress.

The thermodynamic stability of the SMC was studied by *in situ* STM imaging at elevated temperatures. During a prolonged (3.5 h) observation at ∼350 °C, no diffusion of the $n = 4$ clusters was observed. However, 24 out of 137 clusters disappeared from the imaged area. At the same time, noticeable growth of some islands occurred. Figures 7(a) and 7(b) show an example in which two magic clusters ($n = 4$) disappeared and two islands merged between

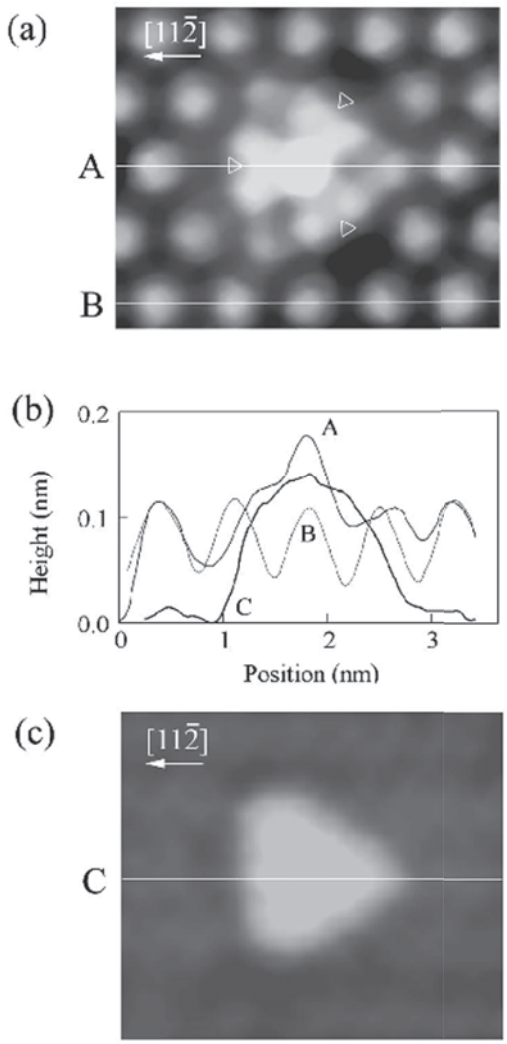

Figure 5. Detailed empty-state (a) and filled-state (c) images (size = 3.3 nm × 2.8 nm) of an $n = 4$ SMC within the $\sqrt{3} \times \sqrt{3}$R30°-reconstructed Ga/Si(111) surface. Triangles indicate the positions of the characteristic vacancies on the surrounding adatom lattice. The tip-height profiles along the three lines indicated are shown in (b).

the two imaging scans separated by 3.5 h. These observations indicate that, when annealed at temperatures beyond ∼350 °C, even the most abundant and stable $n = 4$ clusters show a significant chance of disintegration. This instability at temperatures above 350 °C could be one of the reasons that such SMC escaped the detection of most previous studies in which Ga atoms were usually deposited or annealed at higher temperatures.

2.2. Si magic islands on Si(111)

Homoepitaxy on the Si(111) surface has been extensively studied using various techniques for decades. In particular, the growth of Si on this surface has been a subject under intensive

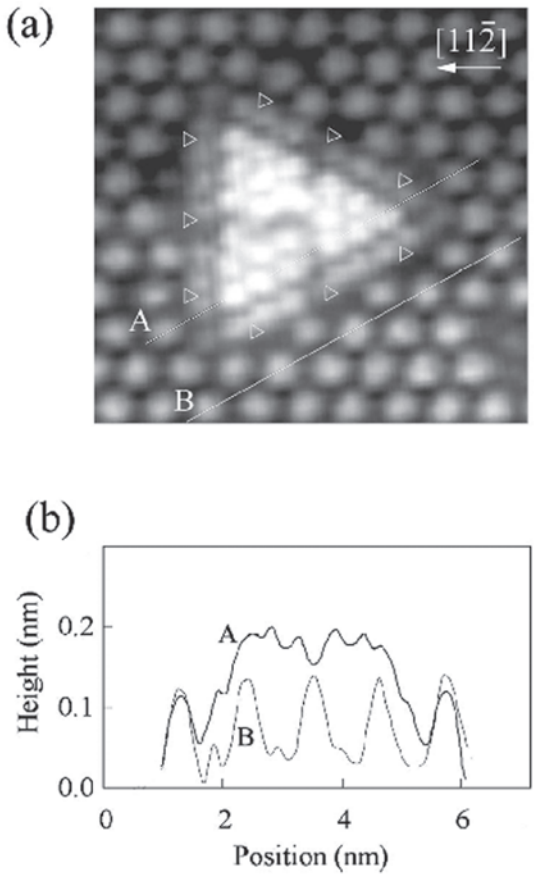

Figure 6. (a) An empty-state image ($V_{tip} = -2.5$ V, $I_t = 2.1$ nA, size = 6.0 nm × 6.3 nm) of a small incommensurate island within the $\sqrt{3} \times \sqrt{3}$R30°-reconstructed Ga/Si(111) surface. Triangles indicate the positions of the characteristic vacancies on the surrounding adatom lattice. (b) Tip-height profiles along the two lines indicated in (a).

investigation since the invention of STM. However, the magic size effect in the islands formed by the deposition of Si was not observed until recently. Again, we will try to recap on the highlights of this experiment and point out the important experimental factors leading to the observation of magic islands in this system.

The key to the successful observation of the magic islands on the Si(111) surface during Si homoepitaxy was the employment of a beetle-type STM in this experiment [33]. The open design of the STM allowed the molecular beam from a Si evaporator to be directed towards the sample while the STM was scanning the growing film. The experiment showed that, during submonolayer (one monolayer or 1 ML was defined as 1.56×10^{15} atoms cm^{-2} in this experiment) growth of Si on Si(111), two-dimensional (2D) islands with Si bilayer thickness (0.31 nm) were formed on the surface. The shape of the islands is triangular, indicating kinetically limited growth shape evolving during growth. Equilibration of these islands without external flux resulted in a transition to a hexagonal equilibrium form [34]. Figure 8(a) shows the Si island size distribution after the deposition of 7% of an atomic layer (sample temperature 725 K, deposition rate 0.5 ML min^{-1}). The size of the islands is plotted

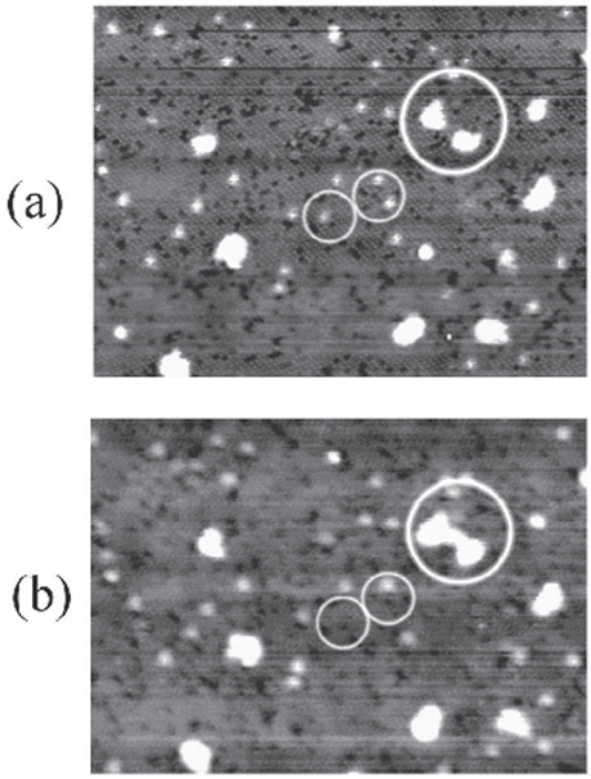

Figure 7. *In situ* STM images showing the disappearance (small circles) of $n = 4$ SMC and merging of islands (large circles) within the $\sqrt{3} \times \sqrt{3}$R30°-reconstructed Ga/Si(111) surface at 350 °C; image (b) was taken 3.5 h after (a).

in units of half a unit cell (HUC) of the well-known Si(111) (7 × 7)-reconstructed surface [35]. Several peaks are observed in the distribution of figure 8(a). The particularly narrow peak at a size of 4 HUC has a $\Delta S/S_{avg}$ of ∼1/4 if ΔS is taken as the full width at half-maximum of the peak.

The observed multiple-peak shape of the island size distribution is quite different from the island size distributions with only one broad maximum observed experimentally for other systems. The typical single-peaked distribution can be explained by assuming that island growth is limited only by the number of adatoms deposited in a 'capture zone' closer to this island than to other islands. The island size distribution is thus similar to the distribution of Voronoi polygons around the islands [36, 37]. Kinetic constraints due to the barriers to attachment of adatoms to the islands on the Si(111) substrate completely change this simple picture.

From a sequence of STM images recording the growth of a selected island as a function of time, as shown in figure 9(a)–9(f), one gets a deeper understanding of the growth kinetics leading to the formation of the Si magic islands. At the beginning of the sequence, as shown in figure 9(a), the shape of the island is a perfect triangle. Later on, as shown in figures 9(b)–9(d), the island has grown by advancement of a row of a certain width along the right island edge. The positions of the kinks at which the row ends are indicated by the arrows in figures 9(b)–9(d). An analysis of the width of this row and further atomically resolved images showed that

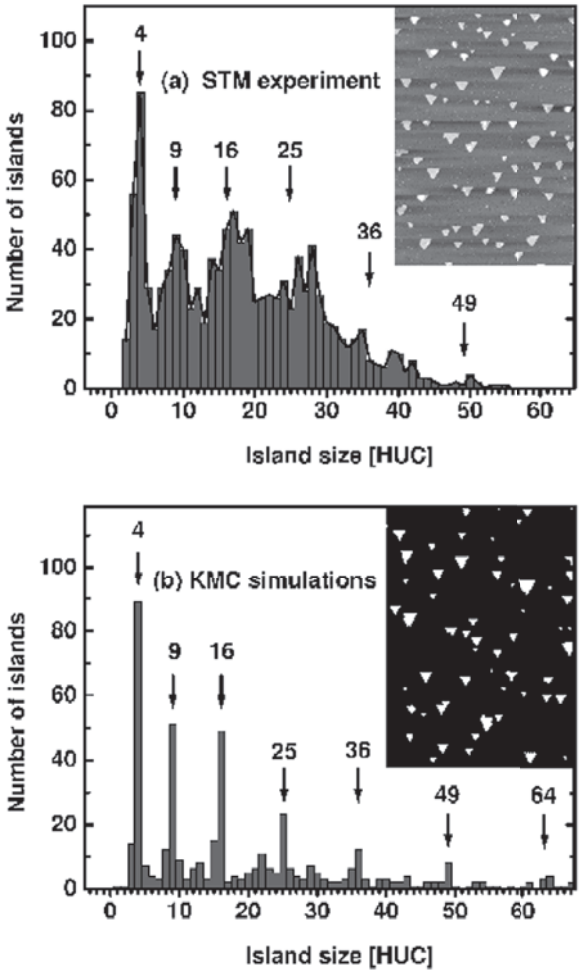

Figure 8. (a) Experimentally observed island size distribution of two-dimensional Si islands grown epitaxially on Si(111) at 7% surface coverage. The distribution consists of several peaks at magic sizes. The size is expressed in half unit cells of the 7×7 reconstruction unit cell. A STM image of the triangular islands is shown in the inset (200×300 nm^2). (b) Island size distribution and the surface morphology (a 100×120 part of a 400×400 lattice is shown in the inset) observed in kinetic Monte Carlo (KMC) simulations. This figure is reproduced from [19] with permission.

the width of such a row is 2.7 nm, which is just the width of one 7×7 reconstruction unit cell. Figure 9(f) shows the completion of a larger 'perfect triangle' towards the end of the growth sequence.

To qualitatively explain the unusual growth kinetics, Voigtländer *et al* [19] suggested that the reconstruction of the surface area surrounding the islands must have played a crucial role in the growth kinetics. Their argument was based on the fact that both the islands and their surrounding surface are made of rhombic 7×7 unit cells that each consist of two triangles. One of these triangles has a stacking fault in the surface layers relative to the substrate stacking (F-HUC) while the other is unfaulted relative to the substrate (U-HUC). During lateral growth of an island, the reconstruction of the surrounding surface area has to be lifted and the substrate atoms have to rearrange to match the bulk structure. It is reasonable to expect different energy

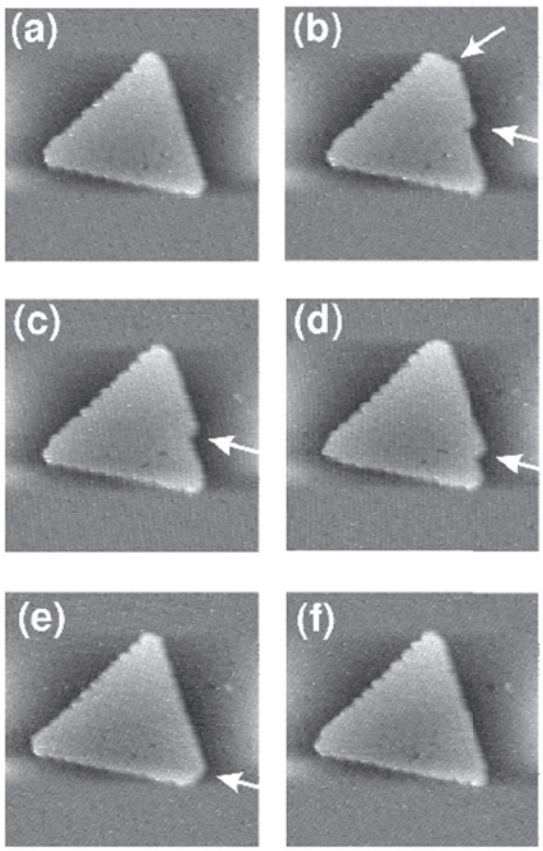

Figure 9. A sequence of images showing the lateral growth of a triangular Si(111) island. A row of the width of the 7×7 unit cell is growing along the right edge of the island in (b)–(f). The image size is 50×50 nm^2; $T = 575$ K. This figure is reproduced from [19] with permission.

barriers for lifting the reconstruction of the U triangle as compared to the F triangle [38]. For the former, only atoms in the uppermost adatom layer have to rearrange. This is associated with a relatively low energy barrier. For the latter, removal of the stacking fault in the layer below the adatoms is needed and therefore requires a larger energy [35]. This should lead to a high activation barrier for overgrowth on the F triangle compared to overgrowth on the U triangle. For perfect triangular islands, i.e., magic islands, areas along the islands' edge are covered by F triangles. Therefore, further lateral growth of magic islands is hindered by the requirement to grow over F triangles with the higher energy barrier. Once an F triangle has nucleated, the neighbouring U triangles can be overgrown more easily (no stacking fault has to be removed). The overgrowth of the next F triangle is facilitated by the existence of a 'macro-kink' (arrows in figure 9). Here the cost of the stacking fault energy is reduced by a gain in the island edge energy: the edge length is reduced after growth of an F triangle. Therefore, neighbouring U and F units can be overgrown in quick succession, leading to the fast growth of a stripe of the width of the 7×7 unit cell. The result of a KMC simulation shows quantitatively very similar island size distribution with pronounced peaks as shown in figure 8(b), and qualitatively very similar growth kinetics, as indicated by the sudden jumps indicated in the evolution of the island size shown in figure 10.

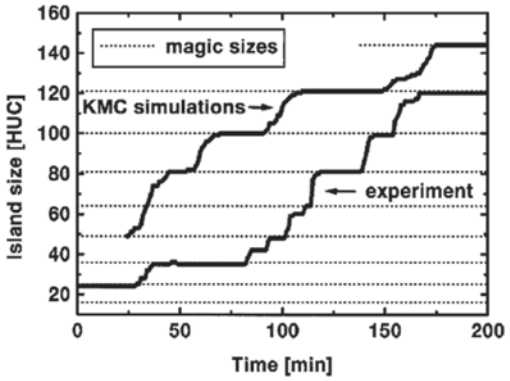

Figure 10. Kinetic Monte Carlo (KMC) and STM results for the evolution of a single island size as a function of time. After rapid growth of rows, longer times without further growth result in plateaus in the time evolution. These plateaus occur just at the magic sizes of perfectly triangular islands. This figure is reproduced from [19] with permission.

In comparison with the SMC in the Ga/Si(111) system, the Si magic island formation on the Si(111) surface has the interesting difference that the triangular shape of the islands is the result of kinetically limited growth. Specifically, the equilibrium shape of the islands at 725 K without the presence of an external Si flux is hexagonal rather than triangular [39]. Such a kinetic magic size effect is different from the thermodynamic magic size effect in the Ga/Si(111) system, where the Ga-induced magic clusters were formed after the sample was annealed at elevated temperatures. Prolonged annealing without the presence of external Ga flux at the formation temperature did not change the structure of the magic clusters, indicating that the SMC of the Ga/Si (111) system are thermodynamically stable.

2.3. Si magic clusters on Si(111)

On deliberately quenching a Si(111) sample from 600 °C to room temperature, clusters of the type shown by the examples in figures 11(a) and 11(b) were formed most abundantly on the (7 × 7)-reconstructed surface [20]. The concentration of such Si SMC was typically of the order of ∼0.01 per 7 × 7 unit cell, but higher concentrations can be achieved by quenching at a faster rate [40]. On samples that were cooled down very slowly, only few clusters were observed. Figure 11(a) shows the filled-state image of two clusters, whose centres appear to be ∼1.5 Å higher than the Si adatoms of the 7 × 7 surface. Figure 11(b) shows the empty-state image of a cluster exhibiting a ring-like structure that consists of six protrusions. Depending on the tip condition, three of the protrusions sometimes appeared brighter as in the case of figure 11(b), and sometimes all of the six protrusions exhibited nearly equal brightness. The solid triangles in figure 11(c) mark the positions of the six protrusions seen in figure 11(b) with respect to the atomic model for the Si(111) 7 × 7 reconstruction [35]. The lateral spacing between the protrusions is ∼3.8 Å, which is much larger than the Si–Si bond length (2.33 Å) in the bulk Si lattice. In view of this, Hwang [40] suggested that such a SMC contains more than six Si atoms. On the basis of the observation of dynamic behaviour of the clusters at step edges, which is to be described later, the magic number is estimated to be between 9 and 15. Although the precise number of atoms and the atomic structure of the magic cluster are yet to be determined, there is probably only one kind of SMC with a definitive magic number rather than several different kinds of SMC in this system [40].

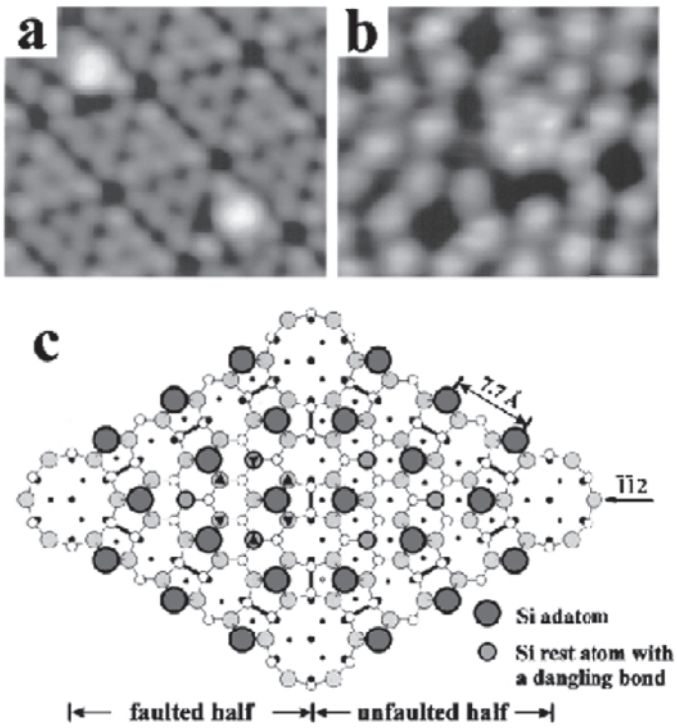

Figure 11. (a) A STM image of two Si magic clusters taken at the sample bias of −1.5 V. (b) An image of another Si magic cluster taken at the sample bias of +1.2 V with a different tip. (c) A model with six protrusions of the cluster seen in (b) marked with triangles. This figure is reproduced from [20] with permission.

The Si magic clusters can withstand temperatures up to 600 °C, but hopping of the clusters occurs too rapidly to be followed by continuous STM scanning at such a high temperature. By measuring the rates for hopping within and out of a faulted or unfaulted HUC at temperatures ranging from 430 to 500 °C, the activation energies and the pre-exponential factors for the hopping motion are determined using the Arrhenius plots shown in figure 12. The activation energies are close to the Si–Si bond strength (∼2 eV) in the bulk. Considering that the cluster may interact with two rest-atom dangling bonds and three Si adatoms in a HUC of the Si(111) (see figure 11(c)), the activation energies for these hopping processes are surprisingly small. Presumably the Si atoms in the clusters are tightly bound; thus their interaction with the substrate is weakened. Hence, Hwang *et al* [20] suggested that a Si SMC diffuses on the surface as a 'unit' with some rather small 'activation energy'. It is not clear, at this point, what the measured 'activation energy' really means, because the apparent hopping of a cluster between two consecutive STM images could be the result of many types of atomic process including dissociation and recombination of atoms. Whether or not the SMC actually 'diffuses' as a 'unit' poses an interesting and challenging fundamental question to both experimentalists and theorists.

Above certain temperatures, the Si SMC are thermodynamically more stable than small bilayer Si islands. When an island decays below a threshold size, it suddenly decomposes into several Si magic clusters. For example, the 5 × 5 island in figure 13(a) was the smallest stable bilayer island observed at 460 °C. Note that there is a disordered unfaulted region around the

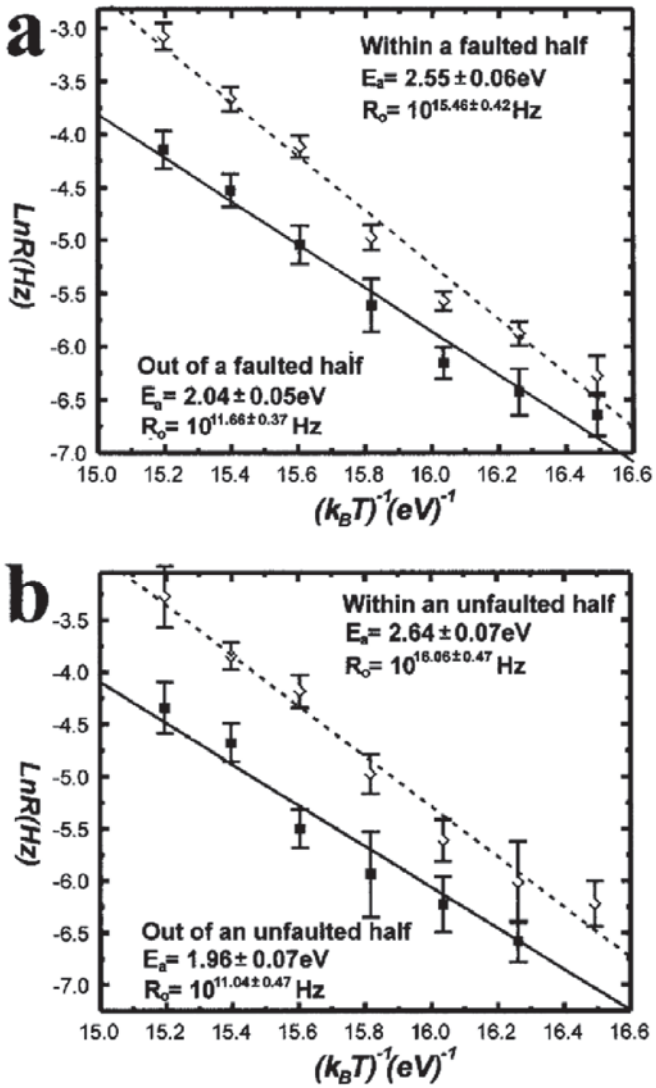

Figure 12. (a) and (b) show Arrhenius plots for the hopping within and out of the faulted and unfaulted half cells, respectively. This figure is reproduced from [20] with permission.

island. It resulted from the decay of a larger island. As time proceeded, the 5×5 island further decomposed into five clusters in the disordered region as shown in figure 13(b). The number of clusters decreased with time (through escaping to the 7×7 region), and the disordered region shrank in size as shown in figures 13(c) and 13(d). Eventually, all clusters disappeared from the imaged region and the disordered area was converted into a perfect 7×7 reconstruction. Similar decomposition of bilayer structures and formation of SMC also take place along the step edges of the Si(111) surface at the temperature of $\sim$450 °C, leading to the fluctuation of the step edges. (By measuring the Si bilayer area disappearing from a step edge and the number of clusters observed in its neighbourhood, the magic number of the cluster was estimated to be between 9 and 15. Such an estimate should be treated with some caution. It tends to be

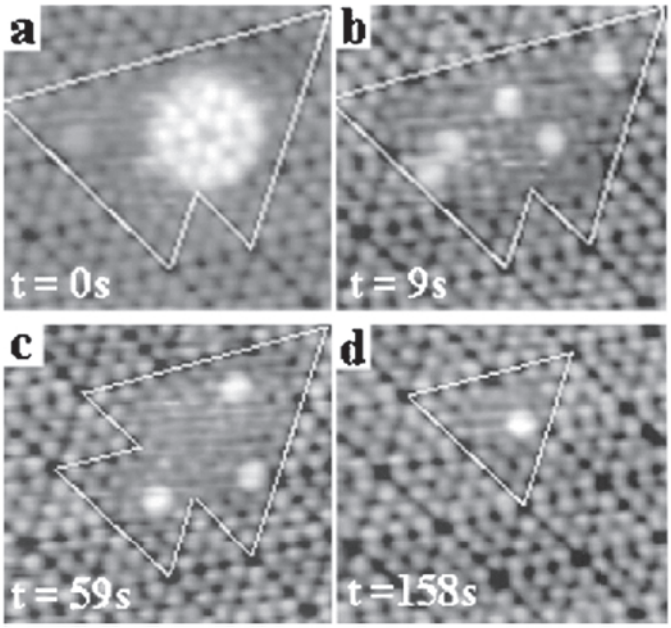

Figure 13. A sequence of STM images showing the decomposition of a 5 × 5 island, taken at the sample bias of −1.5 V. Adatoms in the disordered region (outlined by white lines) are usually very mobile. However, they are less mobile at the outer corner of this region and have a better chance of being seen. This figure is reproduced from [20] with permission.

an overestimate of the size of the clusters because monomers escaping from the region are not detected by the STM imaging.) These observations suggest that the formation energy of the Si SMC and those of the 7 × 7 and 5 × 5 bilayer structures are almost equal in this temperature range.

On cooling samples from 900 °C at a fast rate of >2 °C s^{-1}, a high density of SMC formed and they were trapped in narrow disordered regions at lower step edges and at 7 × 7 domain boundaries, as shown in figure 14. Since the SMC have much higher mobility on 7 × 7 than on the disordered regions, the chances of observing Si clusters as well as their dynamic behaviour on the disordered regions were higher. For samples quenched from temperatures above 900 °C, a small concentration of SMC in 7 × 7 regions as well as a high density of SMC were observed at the domain boundaries, which is similar to the observation by Yang and Williams [41] and others. A high concentration (>0.5 per HUC) of Si SMC can also be produced by depositing Si onto a 7 × 7 Si(111) surface at room temperature and then annealing at ∼350 °C [42]. This indicates that their enhanced stability is of thermodynamic rather than kinetic origin, similar to that of the Ga-induced SMC in the Ga/Si(111) system.

3. Theoretical understanding

Like their experimental counterparts, theoretical studies of two-dimensional (2D) magic clusters either in free space or on surfaces are at a very early stage of development. To our knowledge, only a few studies, some of which are to be discussed in the following, on this subject can be found in the literature. Most of the earlier works examined the magic number of metal clusters. Issues of concern included, for example, the change in the structural stability of

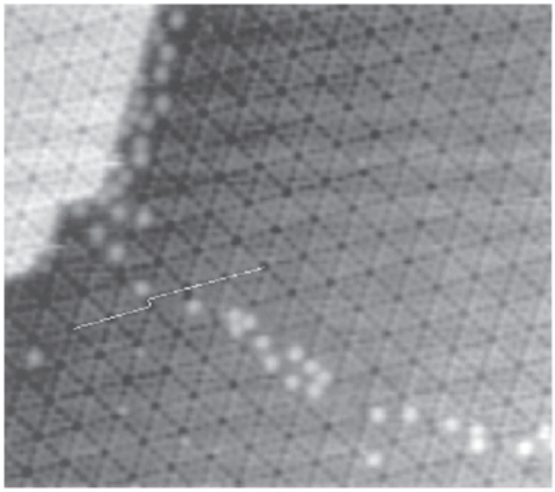

Figure 14. A STM topograph of a surface which is cooled down at the rate $\sim$2 K s^{-1}, taken at 480 °C and the sample bias of −1.5 V. The step edge is fluctuating at this temperature. Most of the magic clusters are trapped at the step edge and the 7 × 7 domain boundary, indicated by the kink of the white line. Two clusters can be seen in the 7 × 7 area. This figure is reproduced from [20] with permission.

a Na_8, which is a 3D magic cluster with an electronic closed shell in free space, as it is brought into contact with a different surface [17]. The study found that on insulating NaCl(001) it remains magic even at 600 K and retains its intrinsic structure. In contrast, Na_8 spontaneously collapses on the Na(110) surface, forming an epitaxial layer. In the following, highlights of some of the theoretical works are reviewed with some emphasis on their relevance to the most recent experiments on SMC.

3.1. Quasi-two-dimensional electron gas clusters

Using density functional theory and the so-called 'ultimate' jellium model [43], the shapes of quasi-2D electron gas clusters were studied. For a completely deformable jellium, the positive ionic background has the same density as the electrons at every point of space, the total charge density being zero. The total energy of the cluster then consists only of the kinetic and exchange–correlation energies of the electrons. The electronic many-body problem can be solved using the Kohn–Sham method with the local density approximation [44]. The ground-state structures of 2D electron clusters were computed using a plane-wave technique that allows a shape relaxation without restrictions. Specifically, a jellium confined between two planar, parallel surfaces of separation $z_0 = 3.9$ au (i.e., the Wigner–Seitz radius of sodium) were examined. By allowing shape relaxation in the (x, y) plane and solving the Kohn–Sham equations iteratively for various forms of the initial potential, the total energies of clusters of various shapes were calculated.

As shown in figure 15, the contours of the self-consistent electron density for quasi-2D electron gas clusters with magic numbers of electrons are either circular or triangular in shape [45]. A systematic study of the 2D ground-state shapes for clusters with up to 34 particles showed that only the triangle and circle appear as closed-shell configurations, whereas other possible shapes of high symmetry, such as a square or pentagon-shaped ground state, have not been seen [46]. Since the sodium magic cluster with strong shell structure is known to be

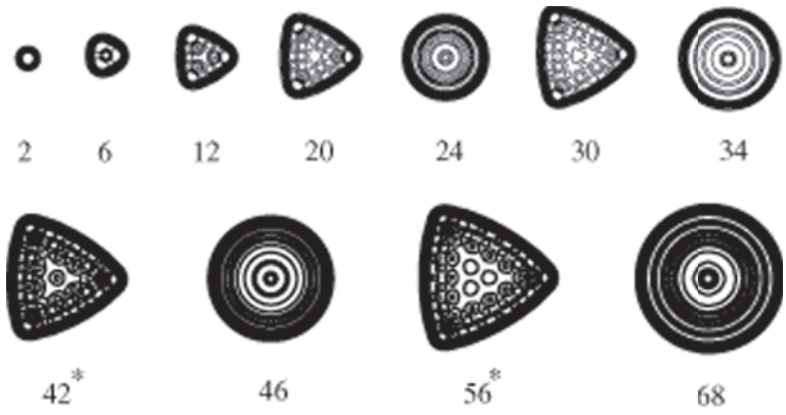

(a)

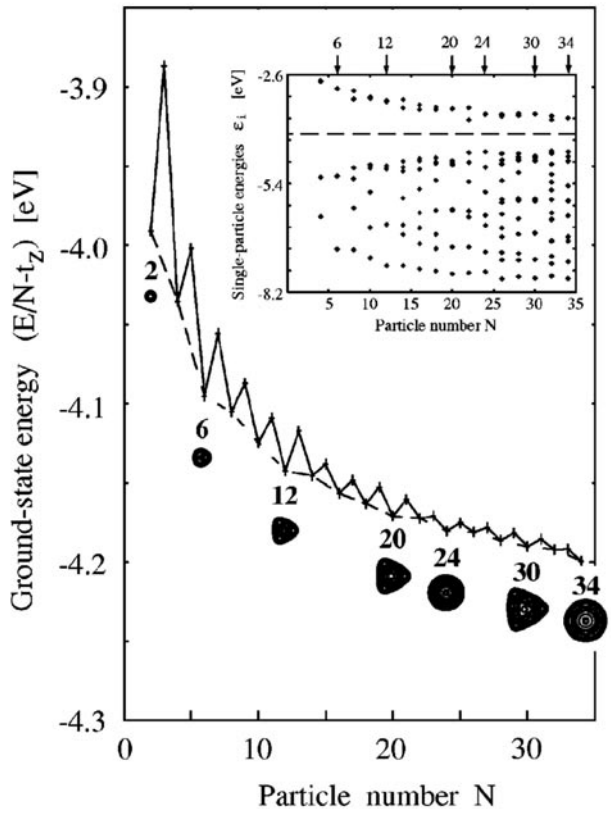

(b)

Figure 15. (a) Contours of the self-consistent densities for quasi-two-dimensional closed-shell clusters. The lowest contour is drawn at 14% of the 2D bulk density. The diameter of the perfect disc with $N = 34$ is $d \sim 33a_0$ (where a_0 is the Bohr radius), giving the length unit in this figure. The stars indicate isomeric states. (b) Ground-state energies per electron, $E(N)/N - t_z$, as a function of size N. Very weak shell closures are found at the magic numbers of both a disc ($N = 2$, 6, 12, 24, 34, ...) and an equilateral triangle ($N = 2$, 16, 12, 20, 30, ...) in two dimensions. Inset: self-consistent Kohn–Sham single-particle energies for even particle number $N = 4$, 6, 8, 10, 12, 20, 22 and 24. The magic shell closures of the circular and triangular shapes are indicated by arrows. This figure is reproduced from [45] with permission.

spherical [47, 48], one would correspondingly expect the magic numbers in 2D to correspond to circular disc shapes for the closed shells with electron numbers 2, 6, 12, 24, 34, ... However, one can see that the ground states of clusters with 6 and 12 electrons are triangular, even though these numbers are 'magic' for a circular disc. The triangular shape for the magic numbers 6, 12, 20 and 30 is obvious from figure 15(a). For bigger sizes the increasing surface energy, which is larger for the triangle than for any other 2D shape, makes non-triangular shapes energetically more favourable. But in all cases studied, the triangular shapes were found as isomers (indicated with stars in figure 15), being only some meV higher in energy than the ground state.

Although not directly applicable, the theoretical study of 2D electron gas clusters provided important information about the formation of SMC. The electronic shell closures of 2D electron gas magic clusters are very 'weak'. That is, the ground-state energy per electron as a function of electron number exhibits very small dips at the closed shells, of the order of a few tens of meV for small clusters to a few meV for larger ones, as shown in figure 15(b). The relatively small enhancements in the stability are further smeared out by the spin-induced odd–even staggering as well as the Jahn–Teller deformation-induced lowering of the ground-state energy for the unclosed systems with even numbers of electrons. In other words, the magic clusters for the 2D electron gas clusters are not very 'magic'. Such weak shell closures are to be expected for a 2D system, as the orbital degeneracy in 2D is much less pronounced than in 3D. From an experimental point of view, such a weak shell closure certainly renders the verification of the existence of 2D magic clusters a big challenge. If one tries to simulate the 2D electron gas clusters by growing monovalent or divalent metal clusters on surfaces, the cluster–surface interaction and the cluster formation temperature have to be considered carefully. For example, a metal cluster on a non-metallic surface is likely to be rather weakly disturbed by the surface. In this case, a 2D metal cluster will tend to assume the geometry preferred by the 2D electron gas. According the above theoretical calculations, for clusters made of divalent elements, triangular clusters are magic both electronically and geometrically. One would expect, for instance, small Mg clusters on a graphite or NaCl(001) surface to prefer the triangular shape if the number of atoms is equal to $n(n+1)/2$, where n is the number of atoms on each side of the triangular clusters. It should be emphasized that this preference for triangular shapes is due to the minimization of the energy of 2D electron gas in the cluster rather than the symmetry of the surface lattice, which has fourfold rather than threefold symmetry. The verification of such triangular 2D magic clusters on a surface without triangular symmetry remains an experimental challenge.

3.2. Magic clusters on surfaces

Due to their intrinsic complexity, numerical calculations of the energetics and structures of clusters on surfaces as a function of cluster size are very scarce. To our knowledge, only the cases of Na on NaCl(100) [17], Pt on Pt(111) [49] and Ag clusters on Ag(100) [50] have been studied systematically. Some calculations addressing the extraordinary stability of the Ga-induced SMCs were conducted soon after their discovery. In the following, the highlights for Ag clusters on Ag(100) and models of the SMC in the Ga/Si(111) system are reviewed with an emphasis on their relevance to the experimental observation of SMC and implications for the growth of monodispersed nanostructures on surfaces.

3.2.1. Ag_i/Ag(100). The energetics of small Ag_i ($i < 4$) clusters on Ag(100) were calculated using the self-consistent Korringa–Kohn–Rostoker (KKR) Green's function method in the local density approximation and using classical molecular dynamics (CMD) simulation based on a

many-body potential due to Finnis and Sinclair and also Sutton and Chen [51, 52]. Since the binding energies for these small Ag clusters (ground states or isomers) calculated by the two methods agree within ∼20%, the CMD method is believed to be reliable. Therefore, the CMD method was used for the calculation of the binding energies of larger clusters up to $i = 12$, which could not be calculated by the KKR method due to the limitation of the computing speed. The calculated equilibrium geometries of the clusters are shown in figure 16. As expected, the results show that clusters of $i = 4$ and 9, with their atomic closed-shell structure on the square lattice of Ag(100), exhibit enhanced binding energies per atom (figure 17) and therefore 4 and 9 can be considered the magic numbers of this system. The enhancements in the binding energy of these magic clusters are, again, of the order of a few tens of meV per atom (similar to those of the 2D electron gas clusters), indicating that the shell closure is also relatively weak in this case of a metal cluster on a metal surface.

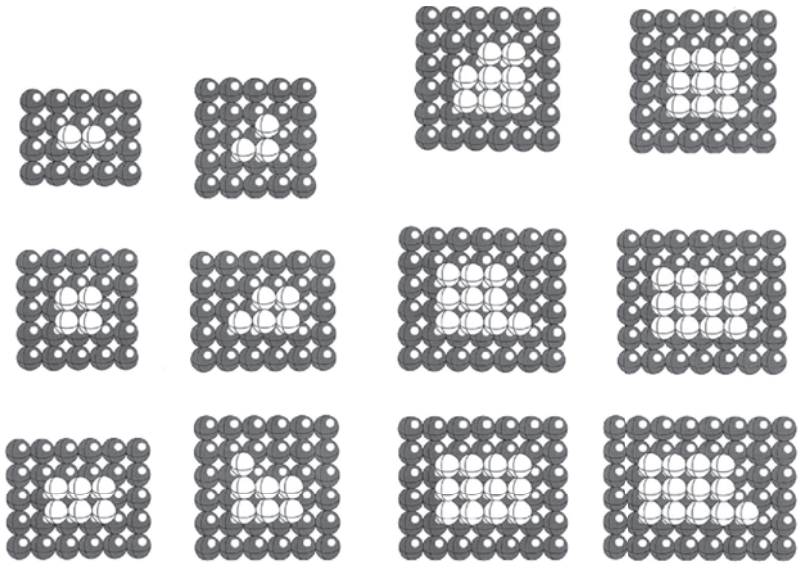

Figure 16. Schematic diagrams of equilibrium geometries of Ag clusters on the Ag(100) surface. This figure is reproduced from [50] with permission.

3.2.2. Ga/Si(111). On the basis of the STM observation of the SMC on the Ga-induced $\sqrt{3} \times \sqrt{3}$R30°-reconstructed Si(111) surface, several atomic models for the most abundant $n = 4$ cluster (decamer) were proposed. In order to verify the validity of the models, theoretical calculations of their energetics were conducted. The first approach is to use a local orbital density functional molecular dynamics method [53] to calculate the total energies of the three models shown in figure 18. The common feature of the models is a Ga decamer embedded within the surface layer of a Ga/Si(111) ($\sqrt{3} \times \sqrt{3}$)-reconstructed surface. The problem is to find whether model (2), which bears the highest resemblance to the STM images of the triangular decamer, is the lowest-energy configuration. The total energies of models (1)–(3) calculated using the single special k-point of Cunningham [54–56] for the hexagonal lattice are −107.097 275, −107.048 681 and −106.993 055 eV/atom, respectively. Model (1) has the lowest total energy. Models (2) and (3) have total energies of 0.215 and 0.46 eV per 1×1 cell, respectively, higher than that of model (1). Therefore, model (2) should not be the structure for the magic $n = 4$ cluster observed by STM.

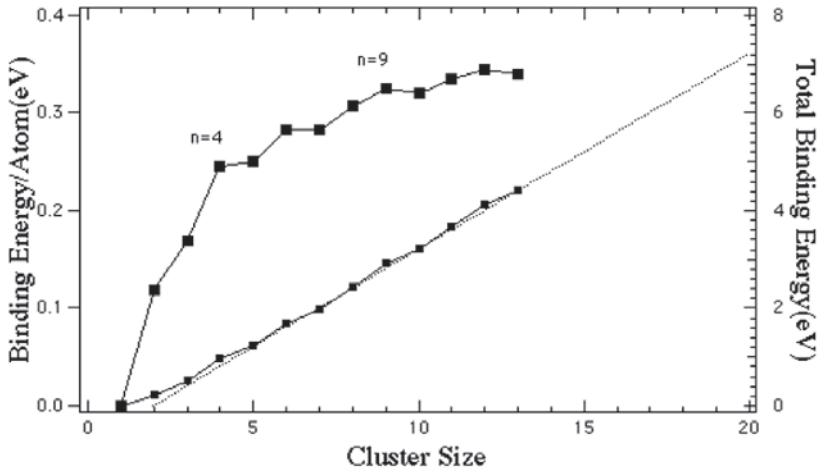

Figure 17. Binding energy as a function of the size of an Ag cluster on Ag(100) according to the calculation of reference [36]. The dashed line is a least-squares fit to the total binding energy. This figure is reproduced from [50] with permission.

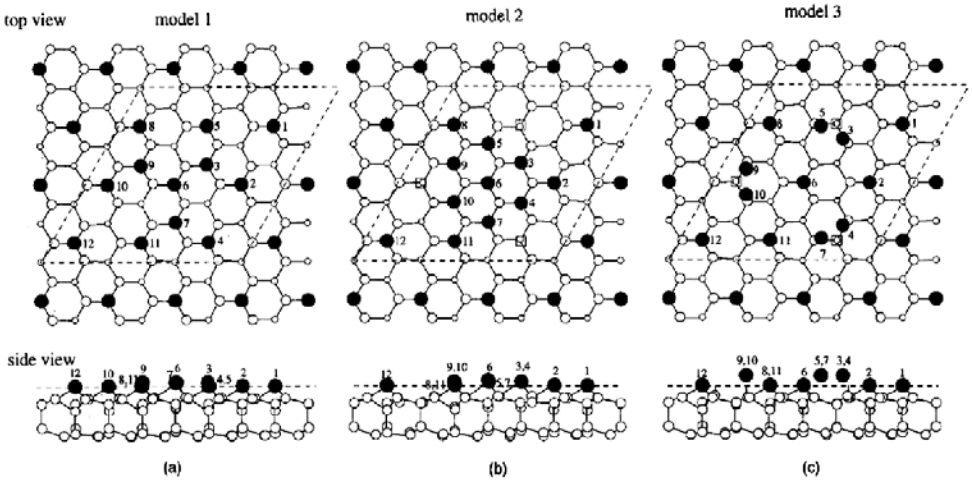

Figure 18. Top and side views of the optimized surface geometry of $n = 4$ (decamer) models considered in reference [53]. (a), (b) and (c) correspond to models (1), (2) and (3), respectively. Filled circles denote the Ga adatoms. Larger and smaller open circles in the top view denote surface and second-layer Si atoms, respectively. Open squares in (b) and (c) represent the missing Ga adatoms of the $\sqrt{3} \times \sqrt{3}$ surface. This figure is reproduced from [53] with permission.

A refined model for the decamer, which can be viewed as a Ga–Si bilayer embedded within the $\sqrt{3} \times \sqrt{3}$ Ga adatom lattice (see figure 19), was proposed [23]. The cluster consists of three and six Ga atoms on the vertices and edges of the triangle, six additional Si atoms (which are presumably invisible under empty-state STM imaging) in the interior and a Ga atom at the centre. The Ga atoms on the vertices and edges have unusual binding configurations. On the inside they are bound to the additional Si atoms; while on the outside they are bound directly to the Si surface, similarly to the adatoms. Such an unusual binding configuration for

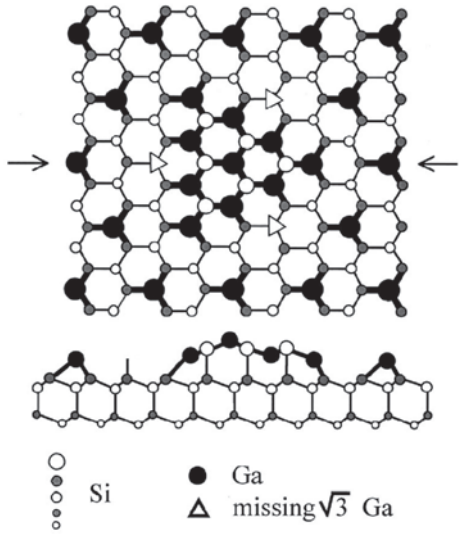

Figure 19. The proposed model for the magic cluster of $n = 4$ shown in figure 5. The lower part shows the cross-section through the indicated region of the cluster.

the edge atoms is qualitatively consistent with the STM observation that they are only slightly higher than the surrounding adatoms. The six additional Si atoms in the interior are located at the atop sites of the Si(111) surface and act as a medium for connecting the Ga atoms in the clusters. Although STM observations have never directly revealed the existence of these additional Si atoms, their presence could better explain the large nearest-neighbour distance ($\sim$0.41 nm) among the atoms of the clusters observed by STM. The Ga atom at the centre is bound to three of six additional Si atoms. It is at the faulted substitutional site belonging to the outer half of the Ga–Si bilayer. Semi-quantitatively, its uniquely higher position is consistent with the observed STM topography.

The proposed model for the $n = 4$ cluster has some characteristics worth noting. First, since all the bonds of its constituent atoms are completely saturated, it can naturally account for the cluster's enhanced stability and orientation preference. Second, the characteristic vacancy pattern in the surrounding adatom lattice can be rationalized because a conflict of binding would occur between an additional Ga atom at the vacancy site (triangles in figure 19) and the side atoms.

An MD calculation based on this Ga–Si bilayer model for the $n = 4$ cluster was conducted to find the positions of the atoms in the relaxed geometry. The results indicate that the six Si adatoms are located approximately at atop sites with lateral deviations within 0.0133 nm, and that the side and vertex Ga adatoms have about 0.015 nm lateral deviations from T_4 sites. The centre Ga atom lies highest among the Ga adatoms, and is higher than the $\sqrt{3} \times \sqrt{3}$ Ga adatoms by about 0.111 nm. The Si atoms lie lower than the central Ga atom by about 0.020 nm. The edge Ga adatoms (3, 4, 5, 7, 9 and 10), which are bonded with two Si adatoms and three Si surface atoms, are higher than the $\sqrt{3} \times \sqrt{3}$ Ga adatoms by about 0.060 nm. The vertex Ga atoms (2, 8 and 11), which are bonded with a Si atom and three Si surface atoms, are higher than the $\sqrt{3} \times \sqrt{3}$ Ga adatoms by about 0.023 nm. These atomic positions are in reasonable agreement with the STM observations of the $n = 4$ cluster. Specifically, the empty-state image showed that the side and centre Ga atoms appear to be higher than the vertex Ga atoms by 0.02

and 0.07 nm, respectively. The filled-state STM image could not resolve height differences for the Ga adatoms, though the centre of the decamer appeared to be higher than the surrounding atoms by 0.12 nm. Another result of the calculation worth noting concerns the absence of Si atoms from the STM images of the $n = 4$ cluster. The images were acquired with a tip bias of 2.5 V, while the fact that the orbital components for the eigenstates are within 2.5 eV above the Fermi level shows that the components of the Si-atop-atom orbital overall are smaller than those of the Ga atoms. Since the Ga atom is much larger than the Si atom, the contribution of the Si adatom to the STM image might be overshadowed by surrounding Ga atoms and was not resolved in the STM measurements.

It is straightforward to generalize the Ga–Si bilayer model for the $n = 4$ clusters to models for other clusters of different sizes. According to this generalized model, the composition of such a triangular cluster can be written as $Ga_{n(n+1)/2}Si_{n(n-1)/2}$, where n is the number of Ga atoms on its side. For $n = 1$, the model corresponds to the case of a single Ga atom of the $\sqrt{3} \times \sqrt{3}$ adatom lattice, which can be treated as a special 'cluster' of monomers. For $n = 2$, there are three Ga atoms on the sides and one Si atom at the centre. For the cluster of $n = 3$, there are six Ga atoms on the sides and three Si atoms in the interior. Due to the lack of second-layer atoms, clusters of $n = 2$ and 3 should be considered as transitional species between monolayer monomers and Ga–Si bilayer clusters. Qualitatively, the proposed models for such transitional species are consistent with the clusters of $n = 2$ and 3 found along the boundaries between degenerate domains of the $\sqrt{3} \times \sqrt{3}$ adatom lattice, as shown in figures 20(a) and 20(b). For $n > 4$, all the clusters described by this generalized model have well-defined bilayer structures. Since clusters of $n = 4$, 5 or 6 are observed while the cluster of $n = 7$ has never been observed, $n = 6$ is likely to be the upper limit for the size of such bilayer clusters. The strain on the Ga–Si bilayer grows with the size of the clusters, and eventually it is released by forming dislocations (domain walls) on the Ga–Si bilayer and results in the creation of incommensurate islands.

Further theoretical support for the Ga–Si bilayer model is found in a density functional study of the structure and stability of $Ga_{n(n+1)/2}Si_{n(n-1)/2}H_{3n+n(n-1)/2}$ clusters ($n = 2$, 3 and 4) [57]. These clusters are conceived to simulate the Ga–Si bilayer model by replacing the cluster–surface connections with Ga–H and Si–H bonds. To further check the influence of the substrate bonding conditions on the cluster structure, $3n$ hydrogens of the Ga–H bonds were replaced with SiH_3 groups and the structure and stability of $Ga_{n(n+1)/2}Si_{n(n-1)/2}(SiH_3)_{3n}H_{n(n-1)/2}$ clusters were examined. The calculations were carried out using the hybrid density functional theory with Becke's three-parameter exchange functional [58] combined with the correlation potential given by Lee, Yang and Parr [59] (B3LYP). The basis sets used are LANL2DZ (Los Alamos National Laboratory effective core potential with a double-zeta basis set for valence electrons) and 6-31G*, both available in the GAUSSIAN 98 program [60] employed in the computations.

In general, the results of the calculation include several features that help us to understand the properties of clusters of this type. Both $Ga_{n(n+1)/2}Si_{n(n-1)/2}H_{3n+n(n-1)/2}$ and $Ga_{n(n+1)/2}Si_{n(n-1)/2}(SiH_3)_{3n}H_{n(n-1)/2}$ clusters ($n = 2$, 3 and 4) are thermodynamically stable and have triangular shape. Their structures consist of fused non-planar Ga_3Si_3 hexagons with three external Si–Ga bonds in the triangle vertices. The Si–Ga bond strength in the clusters is estimated to be 1.74–1.83 eV. In particular, the optimized structures of $Ga_{10}Si_6(SiH_3)_{12}H_6$ under special constraints were calculated in order to facilitate the comparison between theory and the STM observations of the $n = 4$ cluster on Ga/Si(111). Twelve silicon atoms of SiH_3 groups saturating the bonds of three vertex and six edge Ga atoms were put in the same plane forming a triangle surrounding the $Ga_{10}Si_6$ cluster. The Si–Si distance between them, 0.384 nm, corresponds to that in the Si(111) surface. The positions of these Si atoms were

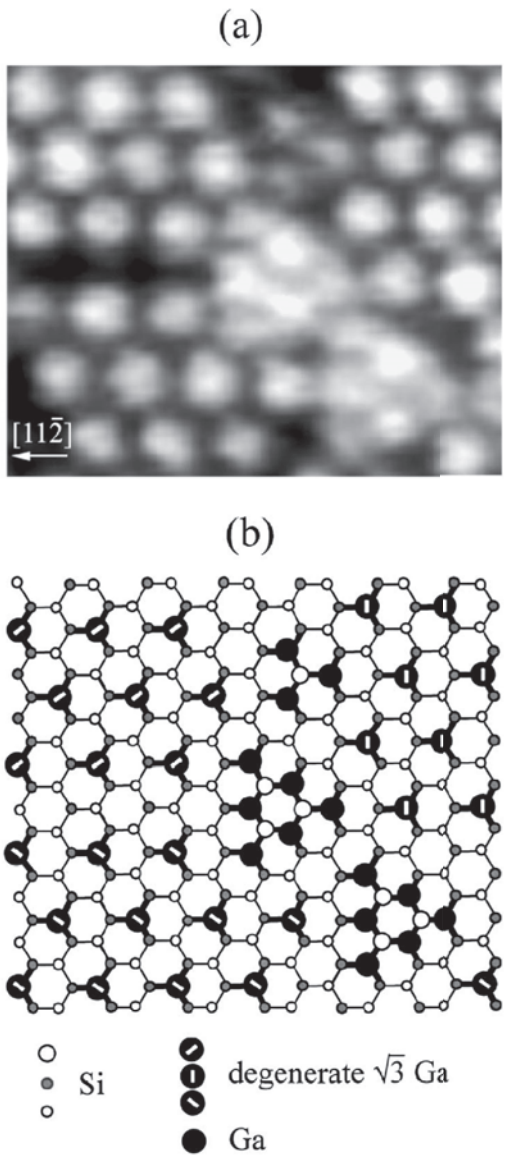

Figure 20. SMC of $n = 2$ and 3 on the Ga/Si(111) surface. (a) An empty-state image ($V_t = 2.2$ V, $I_t = 1.4$ nA, size = 54.3 nm × 33.6 nm) at the boundaries between the degenerate domains of the $\sqrt{3} \times \sqrt{3}$ adatom lattice. (b) Proposed models for these clusters.

frozen during geometry optimization. The resulting structure as shown in figure 21 indicates that the Ga_{edge}–Ga_{edge} distances within a hexagon are longer than the Ga_{edge}–Ga_{edge} distances between different hexagons in the $Ga_{10}Si_6(SiH_3)12H_6$ under constraints.

This result is in line with the STM observations that clearly show that the distances between Ga_{edge} atoms within a hexagon are longer than the distances between Ga_{edge} atoms of different hexagons. Experimentally, the Ga_{edge}–Ga_{edge} distance within a hexagon is 0.58 ± 0.02 nm and the Ga_{edge}–Ga_{edge} distance for atoms in different hexagons is 0.33 ± 0.02 nm, so the difference

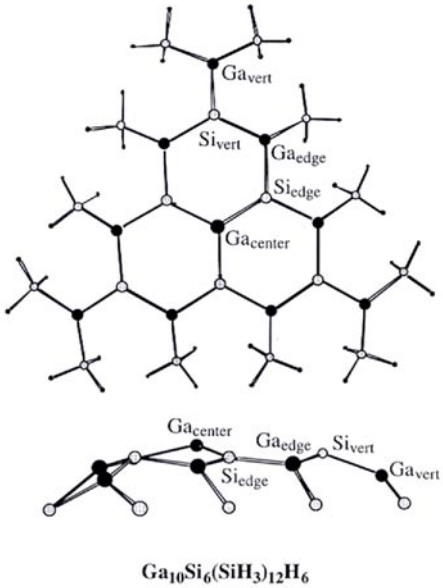

Figure 21. Geometry of the $Ga_{10}Si_6(SiH_3)_{12}H_6$ cluster optimized with boundary constraints. In the side view the hydrogen atoms are not shown for clarity. This figure is reproduced from [57] with permission.

is much more drastic than in our calculations. Such drastic deformation of the hexagon shape can be attributed to the influence of three dangling bonds on the Si(111) surface in the vicinity of the cluster, as shown by triangles in figure 19. The dangling bonds attract the edge Ga atoms pulling them outwards and therefore further increasing the distance between the Ga atoms within a hexagon. Also, the attraction of Ga_{edge} by the dangling bonds can stretch the Ga_{centre}–Ga_{edge} distances (0.44 ± 0.02 nm in STM versus 0.422 nm in calculations). The side view of the calculated (figure 21) $Ga_{10}Si_6$ clusters exhibits characteristics that are quite similar to the experimental observations for the $n = 4$ cluster (figure 5). The central Ga atom lies 0.052 nm above the Si_3 plane made by Si_{edge}; also Ga_{vert} and Ga_{edge} are positioned somewhat below this plane. This also agrees with experimental observations that Ga_{centre} has the highest position as compared with Ga_{vert} and Ga_{edge} which lie at nearly the same level as surrounding silicon atoms. Overall, the calculations enhance our confidence in the Ga–Si bilayer model for the SMC in the Ga/Si(111) system.

4. Effects of SMC on cluster size distribution

The existence of magic clusters in a system modifies the nucleation and cluster growth kinetics and leads to a cluster size distribution different from that predicted by the classical nucleation theory. One of the most important concepts of the theory [61, 62] is the existence of a critical cluster size (i_c). This assumes that clusters of size $i > i_c$ tend to grow rather than decay, whereas for $i < i_c$ decay is more probable. If local equilibrium can be established in a system, then, on the basis of the 'detailed balance' required by the local equilibrium, the concentration of the subcritical clusters can be approximately described by the Walton relation [63]. In terms of the thermodynamic free energy, i_c corresponds to the maximum in the dependence of the free energy on the cluster size, as shown by the continuous line in figure 22. For 2D clusters

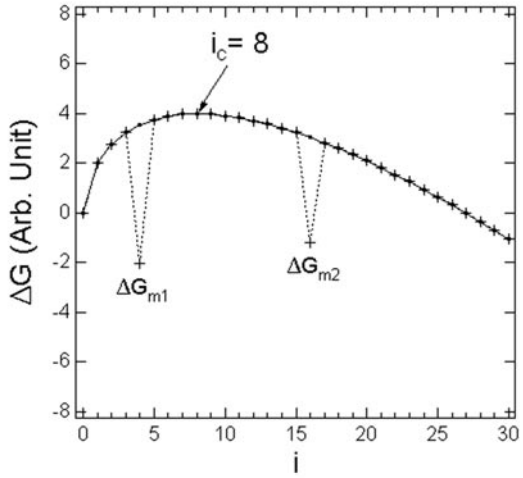

Figure 22. The typical Gibbs free energy as a function of the size of 2D clusters. The dashed line shows the effect of the magic size on the free energy.

of similar shapes on a surface, such a general behaviour of the free energy can be derived from the following equation:

$$\Delta G(i) = -i[\Delta\mu - (\gamma_s + \gamma^* - \gamma_a)\Omega^{2/3}] + i^{1/2}X \tag{1}$$

where $\Delta\mu$ is the supersaturation, γ_s and γ_a are surface free energies of the substrate and adsorbate respectively, γ^* is the free energy of the interface between the substrate and the adsorbate, Ω is the atomic volume of the adsorbate and X is a parameter depending on the edge energy of the cluster [61]. It is be noted that the critical clusters are actually unstable because of their tendency to either grow or shrink in size. According to equation (1), the critical cluster size is

$$i_c = X^2/\{4[\Delta\mu - (\gamma_s + \gamma^* - \gamma_a)\Omega^{2/3}]^2\} \qquad \Delta\mu > (\gamma_s + \gamma^* - \gamma_a)\Omega^{2/3}. \tag{2}$$

It is important to bear in mind that the above macroscopic thermodynamic quantities ($\Delta\mu$, γ_s, γ_a and X) gradually lose their meanings as the size of the clusters reduces. It is not clear whether such macroscopic quantities can be adapted for describing clusters with less than a few hundred atoms. However, for pedagogic convenience, it is helpful to use them to convey the concepts.

Qualitatively, the existence of magic sizes modifies the generally smooth behaviour of the free-energy curve and creates local minima as shown schematically by the dashed lines in figure 22. An important quantitative difference between i_c and i_m is that the former is a local maximum while the latter is a local minimum. In principle, the existence of such a local minimum provides a thermodynamic means for controlling the particle size distribution. In practice, however, both the depth and position of the minimum (i.e. ΔG_m and i_m in figure 22) need to be considered carefully before the magic size effect can be effectively used for controlling the cluster size distribution. Obviously, the deeper the minimum is, the easier the control and the narrower the distribution.

For a given ΔG_m, two types of control strategy can be developed based on the relationship between i_m and i_c. For $i_m < i_c$, the local equilibrium condition and therefore the Walton relation automatically translate the local free-energy minimum at $i = i_m$ into a local maximum in the cluster size distribution. In principle, such an 'equilibrium' approach can be achieved

by carefully controlling the supersaturation ($\Delta\mu$ in equation (2)) and substrate temperature to set $i_m < i_c$. This will ensure that the size distribution of all the subcritical clusters, including the SMC, follows Walton's relation at least approximately. Assuming that the clusters remain in their ground states and the monomers dominate the system, according to Walton's relation the number of i-mers N_i ($i < i_c$) on a surface as a function of their binding energies E_i is

$$N_i/N_0 = (N_1/N_0)^i \exp(E_i/kT) \tag{3}$$

where N_0, k and T are the number of adsorption sites, Boltzmann constant and substrate temperature respectively. Equation (3) is subject to the normalization condition

$$\sum i N_i/N_0 = \theta \cong N_1/N_0$$

where θ ($0 < \theta < 1$) is the total coverage of the adsorbate. In many material systems, the binding energies of adsorbed clusters approach a linear function of i for $i \geqslant i_0$, e.g. that of Ag_i on Ag(100) as shown in figure 17. For such systems,

$$E_i = E_{i0} + \Delta E_b(i - i_0) \qquad i > i_0 \tag{4}$$

where ΔE_b is the binding energy for a monomer binding to a larger cluster. Inserting equation (4) into equation (3) and taking the logarithm of both sides leads to

$$\ln(N_i/N_0) = i[\ln(N_1/N_0) + \Delta E_b/kT)] + (E_{i0} - i_0\,\Delta E_b). \tag{5}$$

When the term inside the square brackets of equation (5) is positive, N_i/N_0 grows exponentially with cluster size i. Therefore, for given ΔE_b, there is a fairly sharp 'condensation' transition temperature at $T_c \cong -\Delta E_b/[k \ln(N_1/N_0)]$, below which the binding energy dominates the entropy effect and all the adatoms tend to aggregate into a single cluster. (It is to be noted that T_c depends explicitly on N_1/N_0, which in turn depends on the total adsorbate coverage through the normalization condition $\sum i N_i/N_0 = \theta$. Therefore for given θ and ΔE_b the exact 'condensation' temperature can only be determined if all the E_i are known.) We see from the above arguments that to use such an 'equilibrium' approach for controlling the cluster size distribution, it is necessary to first keep the substrate temperature above T_c, then quench the system to freeze the 'equilibrium' cluster size distribution. In such an ideal situation, it is straightforward to quantitatively translate a set of E_i into the corresponding size distribution.

For a typical metal/metal system, ΔE_b is of the order of hundreds of meV, e.g. $\Delta E_b = \sim 0.4$ eV for Ag clusters on Ag(100) according to the result of the calculation shown in figure 17 [50]; therefore the T_c are very high for high adsorbate coverage. Just to give some rough idea of the magnitude of T_c and its dependence on θ as well as the effect of magic size, we convert the calculated binding energies of Ag on Ag(100) into the corresponding cluster size distribution. Figures 23(a) and 24(b) show the distribution for $\theta = 0.1$, $T = 1345$ K (60 K higher than the corresponding T_c) and $\theta = 0.001$, $T = 690$ K (20 K higher than the corresponding T_c) respectively. These estimates indicate that, for metal/metal systems, if the shell closure for some magic size is of the order of a few tens of meV, it is unlikely that the magic size effect can be effectively used in the 'equilibrium' approach for creating clusters with very narrow size distribution.

For $i_m > i_c$, the existence of i_m could be, in principle, exploited to modify the cluster growth processes and reduce the cluster size dispersion. Specifically, such a 'kinetic' approach involves using the growth barrier between ΔG_m and ΔG_{m+1} to reduce or even stop the cluster growth. In most thin-film deposition conditions, the typical combination of low temperature and high flux render the supersaturation so large that i_c is usually extremely small ($i_c = 1$ or even 0). Therefore, random nucleation and cluster growth take place simultaneously, leading to a broad and almost flat size distribution ranging from monomers to some large clusters of sizes depending on the growth time. Ideally, it would be possible to take advantage of the growth

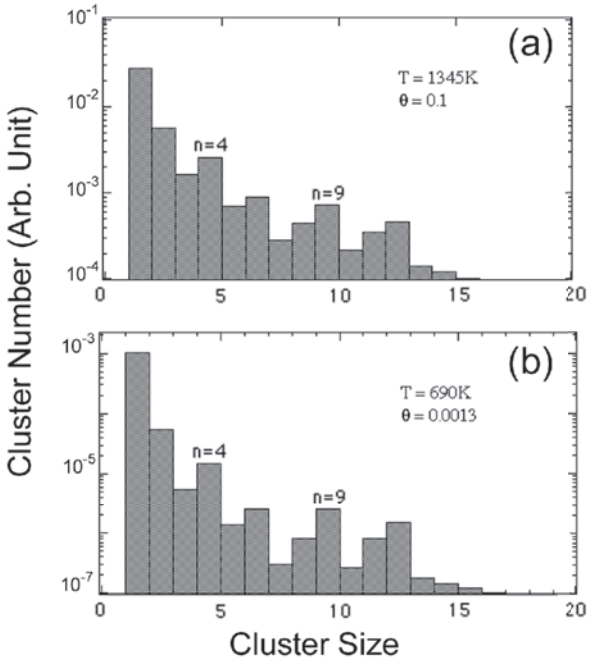

Figure 23. Ag cluster distributions for (a) $\theta = 0.1$, $T = 1345$ K and (b) $\theta = 0.013$, $T = 690$ K, which are estimated from Walton's relation on the basis of the cluster binding energies predicted in [50].

barrier between ΔG_m and ΔG_{m+1} to stop the growth process at $i = i_m$, provided the barrier is high enough. In practice, the barrier heights for most SMC are not likely to be very high. Therefore the challenge is to control the deposition process such that the number of mutually interacting adatoms in any local area is not too much larger than i_m at any time. This would reduce the chance of formation of larger clusters, which are more stable thermodynamically.

One of the schemes for controlling the local concentration of adatoms is that of taking advantage of the periodic or quasi-periodic potential barriers that usually exist on a crystal surface to automatically limit the number of adatoms in a unit cell. With the help of such an upper limit on the local concentration of adatoms, the magic size effect can be exploited more effectively. In fact, such self-organized growth of periodic or quasi-periodic nanostructure arrays with some upper limit on the size distribution on surfaces has been demonstrated in a few systems [12, 64, 65]. By pushing the coverage towards to the corresponding upper limit, it is also possible to use the similar potential barriers provided by the surface as a growth kinetic barrier to squeeze the size dispersion into a narrow range within the upper limit. Since the size distributions of clusters in these systems also exhibit a pronounced peak at a certain size, it is helpful to try to discern the qualitative difference between these 'maximized' clusters and the magic clusters. Figures 24(a) and 24(b) show schematically the free energy as a function of cluster size for a system with some magic size at $i = m$ and that at a 'maximized' size per unit cell, also at $i = m$, respectively. A clear distinction between these two types of cluster is that the former corresponds to a deep free-energy minimum at $i = m$ while the latter corresponds to a sudden drastic increase at $i = m + 1$.

We see from the above analysis that there should exist some systems, at least in principle, whose clusters have a magic size at $i = m$ while the periodic surface potential barriers set

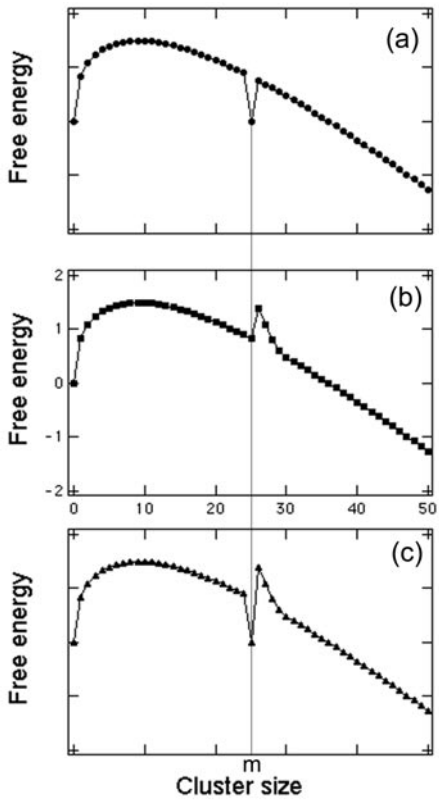

Figure 24. Schematic diagrams showing the free energy as a function of cluster size for (a) a system with a magic size at $i = m$, (b) a system with a growth barrier at $i = m + 1$, (c) a hypothetical system with a magic size at $i = m$ and a growth barrier at $i = m + 1$.

an upper limit for the cluster size at $i = m + 1$, as shown schematically in figure 24(c). Such idealized hypothetical combinations of magic and 'maximized' size effects would provide a more effective pathway to creating clusters with extremely narrow size distribution. Apparently, the effectiveness of this approach depends primarily on the strength of the shell closure, i.e. the depth of the free-energy curve at $i = m$, as well as the height of the barrier between $i = m$ and $m+1$. For example, we are unlikely to find such a pathway on a metal/metal system because of the relative weak closure in such magic clusters, as explained previously. In retrospect, this is consistent with the fact that all of the reported SMCs were observed on semiconductor rather than metal surfaces.

5. Conclusions

The research on SMC is at a very early stage of development. Only three systems with SMC have been identified experimentally, and the theory of SMC remains very rudimentary. We have reviewed the highlights of the experiments with some emphasis on their implications for the fabrication of monodispersed nanostructures. The enhanced stability of SMC can, at least in principle, provide a pathway to controlling the cluster formation process in some selected systems and reducing their cluster size dispersions. The effectiveness of such an

approach depends on the strength of the shell closure at the magic size, which is likely to be weaker on metal surfaces than on semiconductor surfaces. Further experimental and theoretical research on SMC is needed not only to provide fundamental understanding of these unusual self-organized nanostructures with well-defined size and atomic structure but also to pave the way for the exploitation of their quantum properties.

Acknowledgments

We would like to thank Professor T J Chung for encouraging us to write this review. Dr I-S Hwang, Dr B Voigtländer, Dr S M Reimann, Dr M Manninen, Dr P Jena, Dr S-F Tsay and Dr A M Mebel are acknowledged for providing their figures. The preparation of the manuscript would not have possible without the assistance of Ms M F Tsou and Mr N W Liu. This work was partly supported by the National Science Council (NSC 89-2112-M-001-040) of Taiwan, ROC. M Y Lai is supported by a postdoctoral fellowship provided by Academia Sinica.

Note added in proof. The nucleation and growth of Ag clusters on the Pt(111) surface was studied using the molecular dynamics method in [66]. The study found that, at low temperature (400 K) and low coverage (0.1 ML), the cluster size distribution showed apparent magic numbers at $i = 7$ and 10. However, to our knowledge, such magic clusters have not been observed in this material system to date.

References

[1] Tennant D M 1999 *Nanotechnology* ed G Timp (New York: Springer) p 161
[2] Eigler D M and Schweizer E K 1990 *Nature* **344** 524
[3] Heller E J, Crommie M F, Lutz C P and Eigler D M 1994 *Nature* **369** 464
[4] Alivisatos A P 1996 *Science* **271** 933
[5] Wilbur J L and Whitesides G M 1999 *Nanotechnology* ed G Timp (New York: Springer) p 331
[6] Springholz G, Holy V, Pinczolits M and Bauer G 1998 *Science* **282** 734
[7] Black C T, Murray C B, Sandstrom R L and Sun S 2000 *Science* **290** 1131
[8] Brus L 1999 *Nanotechnology* ed G Timp (New York: Springer) p 257
[9] Herman M A and Sitter H 1989 *Molecular Beam Epitaxy (Springer Series in Materials Science vol 7)* (Berlin: Springer)
[10] Jensen P 1999 *Rev. Mod. Phys.* **71** 1695
[11] Bromann K, Félix C, Brune H, Harbich W, Monot R, Buttet J and Kern K 1996 *Science* **274** 956
[12] Brune H, Giovannini M, Bromann K and Kern K 1998 *Nature* **394** 451
[13] Tersoff J, Teichert T and Lagally M G 1996 *Phys. Rev. Lett.* **76** 1675
[14] Shchukin V A and Bimberg D 1999 *Rev. Mod. Phys.* **71** 1125
[15] Knight W D, Clemenger K, de Heer W A, Saunders W A, Chou M Y and Cohen M L 1984 *Phys. Rev. Lett.* **52** 2141
[16] Brack M 1997 *Sci. Am.* **277** 30
[17] Häkkinen H and Manninen M 1996 *Phys. Rev. Lett.* **76** 1599
[18] Lai M Y and Wang Y L 1998 *Phys. Rev. Lett.* **81** 164
[19] Voigtländer B, Kästner M and Šmilauer P 1998 *Phys. Rev. Lett.* **81** 858
[20] Hwang I-S, Ho M-S and Tsong T T 1999 *Phys. Rev. Lett.* **83** 120
[21] Rosenfeld G, Becker A F, Poelsema B, Verheij L K and Comsa G 1992 *Phys. Rev. Lett.* **69** 917
[22] Michely T, Hohage M, Esch S and Comsa G 1996 *Surf. Sci. Lett.* **349** L89
[23] Lai M Y and Wang Y L 1999 *Phys. Rev.* B **60** 1764
[24] Otsuka M and Ichikawa T 1985 *Japan. J. Appl. Phys.* **24** 1103
[25] Zinke-Allmang M and Feldman L C 1987 *Surf. Sci.* **191** L749
[26] Thundat T, Mohapatra S M, Dev B N, Gibson W M and Das T P 1988 *J. Vac. Sci. Technol.* A **6** 681
[27] Zegenhagen J, Hybertsen M S, Freeland P E and Patel J R 1988 *Phys. Rev.* B **38** 7885
[28] Chen D M, Golovchenko J A, Bedrossian P and Mortensen K 1988 *Phys. Rev. Lett.* **61** 2867
[29] Patel J R, Zegenhagen J, Freeland P E, Hybertsen M S, Golovchenko J A and Chen D M 1989 *J. Vac. Sci. Technol.* B **7**

[30] Köhler U, Demuth J E and Hamers R J 1989 *J. Vac. Sci. Technol.* A **7** 2860
[31] Zegenhagen J, Patel J R, Freeland P, Chen D M, Golovchenko J A, Bedrossian P and Northrup J E 1989 *Phys. Rev.* B **39** 301
[32] Hammers R J 1989 *Phys. Rev.* B **40** 1657
[33] Voigtländer B, Zinner A and Weber T 1996 *Rev. Sci. Instrum.* **67** 2568
[34] Mysliveček J, Jarolmek T, Šmilauer P, Voigtländer B and Kästner M 1999 *Phys. Rev.* B **60** 13 869
[35] Takayanagi K, Tanishiro Y, Takahashi S and Takahashi M 1985 *Surf. Sci. Lett.* **164** 367
[36] Mulheran P A and Blackman J A 1996 *Phys. Rev.* B **53** 10 261
[37] Bartelt M C and Evans J W 1996 *Phys. Rev.* B **54** R17 359
[38] Shimada W and Tochihara H 1994 *Surf. Sci. Lett.* **311** 107
[39] Köhler U, Andersohn L and Dahlheimer B 1993 *Appl. Phys.* A **57** 491
[40] Hwang I-S 2000 private communication
[41] Yang Y-N and Williams E D 1994 *Phys. Rev. Lett.* **72** 1862
[42] Lai M Y and Wang Y L 2001 unpublished
[43] Koskinen M, Lipas P O and Manninen M 1995 *Z. Phys.* D **35** 285
[44] Kohn W and Sham L J 1965 *Phys. Rev.* A **140** 1133
[45] Reimann S M, Koskinen M, Häkkinen H, Lindelof P E and Manninen M 1997 *Phys. Rev.* B **56** 12 147
Reimann S M, Koskinen M, Helgesson J, Lindelof P E and Manninen M 1998 *Phys. Rev.* B **58** 8111
[46] Reimann S M, Koskinen M, Lindelof P E and Manninen M 1997 *Z. Phys.* D **40** 310
[47] Ekardt W 1984 *Phys. Rev.* B **29** 1558
[48] Hintermann A and Manninen M 1983 *Phys. Rev.* B **27** 7262
[49] Fallis M C, Daw M S and Fong C Y 1995 *Phys. Rev.* B **51** 7817
[50] Nayak S K, Jena P, Stepanyuk V S, Hergert W and Wildberger K 1997 *Phys. Rev.* B **56** 6952
[51] Finnis M W and Sinclair J E 1984 *Phil. Mag.* A **50** 45
[52] Sutton P and Chen J 1990 *Phil. Mag. Lett.* **61** 139
[53] Tsay S-F, Tsai M-H, Lai M Y and Wang Y L 2000 *Phys. Rev.* B **61** 2699
[54] Cunningham S L 1974 *Phys. Rev.* B **10** 4988
[55] Tsai M-H, Dow J D and Sankey O F 1992 *Phys. Rev.* B **46** 10 464
[56] Tsai M-H and Hass K C 1995 *Phys. Rev.* B **52** 16 420
[57] Mebel A M, Lai M Y and Wang Y L 2000 *Chem. Phys. Lett.* **318** 27
[58] Becke A D 1993 *J. Chem. Phys.* **98** 5648
[59] Lee C, Yang W and Parr R G 1988 *Phys. Rev.* B **37** 785
[60] Frisch M J *et al* 1998 *GAUSSIAN 98*
[61] Venables J A, Spiller G D T and Hanbücken M 1984 *Rep. Prog. Phys.* **47** 399
[62] Brune H 1998 *Surf. Sci. Rep.* **31** 121
[63] Walton D 1962 *J. Chem. Phys.* **37** 2182
[64] Vitali L, Ramsey M G and Netzer F P 1999 *Phys. Rev. Lett.* **83** 361
[65] Chambliss D D, Wilson R J and Chiang S 1991 *Phys. Rev. Lett.* **66** 1721
[66] Blandin P, Massobrio C and Ballone P 1994 *Phys. Rev.* B **49** 16 637